Scientific Research Publishing

Journal of Modern Physics, 2026, 17(8), 940-952
https://www.scirp.org/journal/jmp
ISSN Online: 2153-120X
ISSN Print: 2153-1196

Electronic Thermal Conductivity of UN Revisited

Barbara Szpunar[1*], Sergei L. Dudarev [2]

[1]Department of Mechanical Engineering, University of Saskatchewan, Saskatoon, SK, Canada
[2]Atomic Energy Authority, Culham Centre for Fusion Energy, Oxfordshire, UK
Email: *Barbarausask@gmail.om

How to cite this paper: Szpunar, B. and Dudarev, S.L. (2026) Electronic Thermal Conductivity of UN Revisited. *Journal of Modern Physics*, **17**, 940-952.
https://doi.org/10.4236/jmp.2026.178042

Received: June 17, 2026
Accepted: August 22, 2026
Published: August 25, 2026

Abstract

Recently, we demonstrated that the electronic thermal conductivity of UN can be predicted from first principles, in good agreement with experimental measurements. Furthermore, we found that by implementing Hubbard U (HU) or spin orbit (SOC) corrections and antiferromagnetic (AFM) ordering was necessary to increase electrical resistivity and reduce the previously overpredicted electronic thermal conductivity for non-magnetic UN. We found that calculated electronic thermal conductivity for 3k noncollinear (NCL) magnetism in UN was underpredicted with and without SOC correction. Additionally, thermomechanical properties were presented at finite temperatures as calculated using quasi-harmonic approximation (QHA) within Density Functional Theory (DFT).

Keywords

UN, Thermal Conductivity, Thermal Expansion, Bulk Modulus, DFT, QHA2

1. Introduction

Metallic ceramic fuels, for example, UN, are very interesting materials as their thermal conductivity remains high even at very high temperatures due to significant electronic heat transport [1]. U-density (34.2 atoms/nm^3) in UN is higher than in UO_2 (24.47 atoms/nm^3); therefore, it is more economical and suitable for implementation as a lower enrichment (LEU) fuel. They are important because urania fuel, which is used in conventional nuclear reactors, is not the optimum option for some designs of new-generation reactors due to its low thermal conductivity [2].

There have been many fewer investigations of UN than UO_2, since Uranium

was used in conventional nuclear reactors. However, due to the presence of U atoms in both compounds, similar techniques can be used. In particular, Hubbard U is widely used with various implementations [3] [4]. Lichtenstein *et al.*'s updated implementation has also been successfully used for UO_2 with $3k$ noncollinear magnetism, as described in detail [4] [5]. We use HU in the rotationally orbital-invariant implementation, (Dudarev *et al.* [4]). It has been found previously [6] that the results of the energy of formation of defects and band gaps of UO_2 with the HU implementation were inconsistent due to the presence of multiple metastable states. Although the energetics of the system may be significantly affected by metastable states, the structural parameters remain nearly unchanged [6].

These metastable states originate from different ways of filling the seven 5f levels of U with two electrons [6], which can be trapped there. The occupation matrix control code (OMC) [7] is now widely used to select states during several initial iterations to avoid trapping in a metastable state. Although this method still does not provide exact energetics due to spin orbit (SOC) corrections being neglected, it leads to consistency between various calculations [6]. It has been reviewed recently [8] that while OMC can perhaps reach the true ground state of bulk materials more reliably, the U-ramping method is more popular for the calculation of defects. Furthermore, in UO_2, the increased number of degrees of freedom [8] and additional splitting (Dr. S. L. Dudarev's private communication) when SOC correction is implemented reduce the possibility of falling into a metastable state. Therefore, unless specified, it can be assumed that SOC correction is enough to achieve the ground state without applying OMC [8], and we implemented them here for comparison.

2. Methodology

The new electron-phonon physics from first principles code Electron-Phonon coupling using Wannier functions (EPW, v. 5.4) code [9], as implemented in Quantum Espresso (QE, v. 6.8) code [10] based on density-functional theory (DFT), predicts electronic-thermal conductivity for thorium mononitride and thorium carbide in agreement with experiment. However, the current version of the EPW code for non-magnetic solids overestimates the electronic thermal conductivity of UN and underestimates resistivity [11]. Therefore, recently, we evaluated the relaxation time for UN from the EPW code and implemented it into the new BolTztrap2 code [12] combined with the VASP code [13], which allowed us, to calculate the electronic transport of magnetic UN with the additional implementation of Hubbard U [4] solely from first principles [11].

The absolute value of the electrons' relaxation time ($\tau_{800} = 6.70 \times 10^{-15}$ s) was evaluated using non-magnetic thermal electronic conductivity calculated at 800 K temperature from the BoltzTraP2 code (in relaxation time units: 4.08677×10^{15} $W \cdot m^{-1} \cdot K^{-1} \cdot s^{-1}$) and calculated from solving the Boltzmann transport equation

(BTE) implemented in the EPW code (27.39717 $W \cdot m^{-1} \cdot K^{-1}$) at the same temperature [11]. We adapted the scattering rate determined earlier (using the EPW code), increasing linearly with temperature ($ds_R/dT = 1.23373 \times 10^{11}\ s^{-1} \cdot K^{-1}$), for the selected 6, 7 bands within the $k_B T$ energy range around the Fermi Energy ([14], Fig. 7). The derived correlation for electrons' relaxation time (τ_T) as a function of temperature is [11]:

$$\tau_T = \left(\tau_{800}^{-1} + (T-800)\,ds_R/dT\right)^{-1} = \left(1.4917\times10^{14} + (T-800)1.23373\times10^{11}\right)^{-1} \quad (1)$$

We assumed that the derived electrons' relaxation time (Equation (1)) for non-magnetic (NM) UN is the same for the previously studied ferromagnetic (FM) and antiferromagnetic (AFM) UN. The same electrons' relaxation time was used in this study for the noncollinear (NCL) magnetic structure with and without SOC incorporated to investigate electronic thermal conductivity. However, it is important to expand EPW code to include magnetic cases to verify this assumption.

We used DFT + Hubbard U in the rotationally orbital-invariant implementation to develop the correlation ($R^2 = 0.99$) between band gap and Hubbard U (in eV) in UO_2 [15]:

$$G = 0.0109\,U^2 + 0.5268\,U \quad (2)$$

Furthermore, we found [15] that Hubbard U of 3.5 eV reproduced the experimentally measured band gap of ~2 eV in UO_2, and therefore we used this value for UN for a material-transferability assumption. Similarly, Dudarev *et al.* [5] found the value of HU = 3.46 eV computed fully by *ab initio* that delivers the band gap of 2.11 eV in UO_2. HU = 3.46 eV was used in recent studies of noncollinear 3*k*-type antiferromagnetic UN by Li *et al.* [16]. It has also been noted that in the literature multiple values of HU in the range from 1.0 eV - 5.0 eV were employed for UO_2 and UN. We find that various HU values are required to reproduce the respective properties.

The generalized gradient approximation (GGA) of Perdew, Burke [17], and Dudarev Hubbard U [4], the rotationally orbital-invariant implementation in the VASP code (option 2) [13], was used. Density functional method (DFT) was used here with the most recent (version 64) generalized gradient approximation (GGA) potentials [17] that are based on the projector-augmented-wave method projector-augmented-wave (PAW) as implemented in VASP code [13]. The energy cutoff for the plane-wave basis was set to 500 eV.

Furthermore, we explored the lattice constant, bulk modulus and its derivative over pressure, and the thermal expansion of UN at non-zero temperatures using the quasi-harmonic approximation (QHA) implemented in Phonopy combined with VASP [18] [19]. The accurate calculations of energy versus volume with a fine grid of (12, 12, 12) k points were required to resemble a parabolic fit for the energy versus volume relation (*e-v*.dat file). The properties of AFM UN with and without HU and SOC corrections versus UN with noncollinear magnetic ordering

with and without spin-orbit correction included were compared.

The thermal expansion is studied using various definitions, and here we use the linear thermal expansion coefficient (α) equal to one-third of the volume thermal expansion evaluated in Phonopy:

$$\alpha = a^{-1}\,\mathrm{d}a/\mathrm{d}T \tag{3}$$

which is defined for QHA for temperatures $0 \leq T \leq 1000$ K. The temperature step is set to 50 K with $\alpha = 0$ K^{-1} at 0 K.

Additionally, we present comparison between mean coefficient of linear thermal expansion (*MCTE*, $T_0 = 303$ K) and extrapolated a calculated from experimentally measured lattice constant Equation (3) of UN in oxidative temperature:

$$MCTE = \frac{a - a_0}{a_0\left(T - T_0\right)} \tag{4}$$

The elastic constants were evaluated using the elastic code [20] (Release v5.1.0-14-g6596fd4) with a command option and adapted for a high-performance batch submission script posted on our research web page.

T_M, melting point temperature, was calculated using an empirical correlation:

$$T_m = 553 + 5.91C_{11} \tag{5}$$

3. Results

In Table 1 and Table 2, we summarise our results calculated using the methodology described in Section 2. The initial magnetic moment was set to 1 μ_B along z direction for 1 k antiferromagnetic (AFM) state and 0.5 along respective x, y, z coordinates for noncolinear (NCL) magnetism in UN.

In Table 1, lattice constant (forced $a = c$), electrical resistivity (ρ), and conductivity (κ_e) are listed as calculated at 300 K (row 3 - 8) versus experimental results listed in row one. In the last three column spin, orbital and total moments are listed versus experimental magnetic moment measured below the Neel temperature [21] listed in row two. The calculated *Ms* values are larger than the shown value of 0.75 μ_B, but smaller than the value evaluated from the susceptibility effective moment (2.8 μ_B).

We found that employing both SOC and HU correction leads to unphysically high resistivity therefore we do not include these results as further investigation is required. The initial diagonal occupation matrix was set by VASP automatically the same for AFM with SOC or HU correction included.

In Table 2, we compare experimental values of single-crystal elastic constants (C_{ij}) [17] (listed in the second row) versus those calculated using VASP [13] and the elastic code [20]. We found a reasonably good agreement for GGA/PBE calculations for NM and AFM UN. However, for AFM and NCL cases, using GGA/PBE with HU or SOC correction incorporated, C_{11} elastic constants were underestimated. Note that we managed by enhancing accuracy to fix incorrect elastic constants for

AFM UN, GGA + HU [11], which are corrected in Table 2, row five. We present here the C_{11} elastic constant, which is reduced by the HU = 3.5 eV or SOC correction implementation for AFM UN or NCL UN.

Table 1. The calculated at 300 K versus experimental values of lattice constants (a, c) electrical resistivity (ρ), thermal electronic conductivity (κ_e), and at 0 K, the value of spin-induced magnetic moment (M_S) and orbital moment (M_L), $M_T = M_S + M_L$, per U atom in UN cell or in the bracket magnetic moment of 5f electrons per U in various magnetic states (NM—non-magnetic, 1k AFM—antiferromagnetic, 3k NCL - noncolinear) of UN. The GGA/PBE functional was used except where indicated incorporation of GGA with HU = 3.5 eV or SOC correction. The listed experimental references are in order as presented values in row 2.

UN magnetic state	a/c [nm]	ρ [Ωm]	κ_e [W·m^{-1}·K^{-1}]	$M/_S$ [μB]	$M/_L$ [μB]	$M/_T$ [μB]
Experiment [21]-[23]	0.4889	1.46×10^{-6}	5.03			0.75
NM	0.4853	4.68×10^{-7}	15.66	0	0	0
AFM	0.4860	6.34×10^{-7}	11.56	(0.94)	0	(0.94)
AFM (HU: 3.5 eV)	0.4960	8.95×10^{-7}	8.19	(1.28)		(1.28)
AFM (SOC)	0.4878	1.19×10^{-6}	6.19	0.86	−0.95	−0.09
NCL	0.4880	2.77×10^{-6}	2.65	1.09		1.09
NCL (SOC)	0.4883	2.80×10^{-6}	2.62	1.02	−1.47	−0.46

Table 2. Calculated versus experimental values of single-crystal elastic constants (C_{ij}) at 0 K. The shown melting point T_m is calculated from C_{11} using Equation (5). Calculated via DFT/QHA bulk modulus (BM), its derivative over pressure (BM'), and linear thermal expansion coefficients at 300 K are shown in the last column.

UN magnetic state	C_{11} [GPa]	C_{12} [GPa]	C_{44} [GPa]	T_M {K}	BM (300 K) [GPa]	BM' (300 K)	α (300 K) [10^{-6} K^{-1}]
Exp. [21] [22] [24]	423.9	98.1	75.7	2923 ± 100	203205.9	6.30	7.5210
NM	430.8	132.4	42.3	3099	228.8	4.28	4.4224
AFM	408.7	126.8	50.4	2968	209.6	4.78	4.4224
AFM (HU: 3.5 eV)	339.4	95.4	63.05	2559	170.4	5.11	6.5664
AFM (SOC)	372.0	118.6	49.4	2751	195.9	4.58	5.1303
NCL	369.2	130.6	50.23	2735	209.0	4.62	4.9015
NCL (SOC)	375.9	113.8	55.47	2775	194.2	4.44	4.9015

T_M, melting point temperature, was calculated using empirical correlation (Equation (5)).

The shown in Table 2 experimental value for the linear thermal expansion coefficient (α) was derived using Equation (3) and the published correlation for a lattice constant of UN as a function of temperature [24]. Interestingly, we get the best agreement with experiment for BM' and α using GGA + HU equal 3.5 eV, while bulk modulus (BM) is in the best agreement with experiment for GGA without HU and SOC corrections.

3.1. Resistivity

In Figure 1 we compare experimental resistivity [24] versus electrical resistivity calculated by combined BltzTrap2/VASP codes with relaxation time evaluated by Equation (1). The results for NM, $1k$ AFM and $3k$ NCL UN with GGA and with and without HU and SOC correction incorporated are shown as indicated. The best agreement with experiment, indicated by the black open circle, is for $1k$ AFM UN resistivity calculated using GGA with HU equal to 3.5 eV or SOC corrections (solid dark red circles) incorporated. The presence of NCL magnetism significantly increases resistivity, while the results for NM UN underestimate it as can be compared in Figure 1.

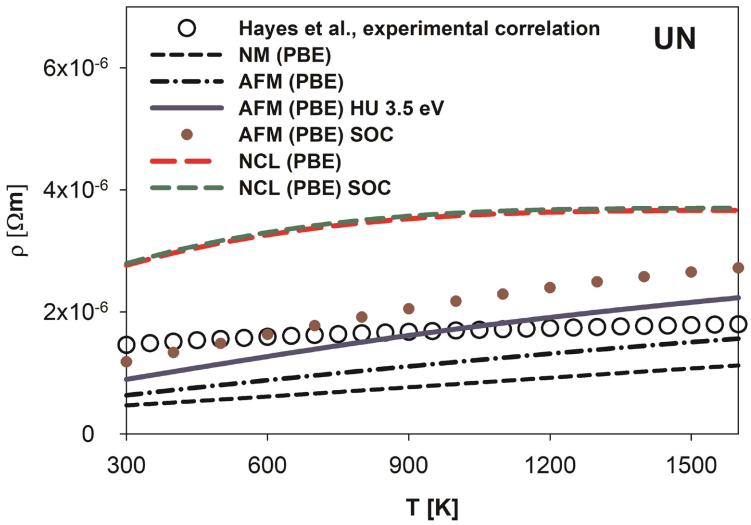

Figure 1. The comparison of the experimental electrical resistivity of UN (indicated by the open black circles) [24] against the calculated values using BoltzTrap2 code with electrons' relaxation time evaluated from Equation (1). The evaluated resistivity for GGA calculations for NM UN is indicated by a black short-dashed line, and a dashed dot black line for AFM UN. GGA + HU results are displayed by a solid dark blue line. NCL UN case is indicated by a long-dashed red line for GGA calculations and for GGA with SOC correction by a green dashed medium line.

3.2. Conductivity

In Figure 2, the respective results are shown for electronic thermal conductivity calculated using the Wiedemann-Franz law as described before [e.g. 11] and listed in Figure 1 resistivity. Universal Sommerfeld Lorenz number was used, which is widely used for modeling nuclear fuel at operating conditions and reliable for 5f electrons at these higher temperatures. The same respective display as for ρ is used. We compare these results with the previously presented [11] κ_e and obtained using the EPW code (dashed-dot-dot black line) and previous estimates by Czekała *et al.* [25] and Yin *et al.* [26] and indicated by solid triangles up and down, respectively. Surprisingly, our new calculations for AFM UN calculated using GGA with SOC correction included (displayed by dark solid red circles) agree even better with the previous evaluations [25] [26] than when the

HU = 3.5 eV correction (indicated by a solid dark blue line) is included. NCL UN case with and without SOC correction underestimates thermal conductivity. The combined calculations with both HU and SOC corrections included are not included due to observed significant overestimate of resistivity and therefore reduction of electronic thermal conductivity, respectively. Further investigation is required. All results calculated with the relaxation time calculated using Equation (1) and combined BoltzTrap2/VASP codes show correctly increasing κ_e with temperature, which is in contrast to the decrease in κ_e at lower temperature when using the EPW code for NM UN and indicated by the dashed-dot-dot black line. The results are very consistent between having implemented HU or SOC correction.

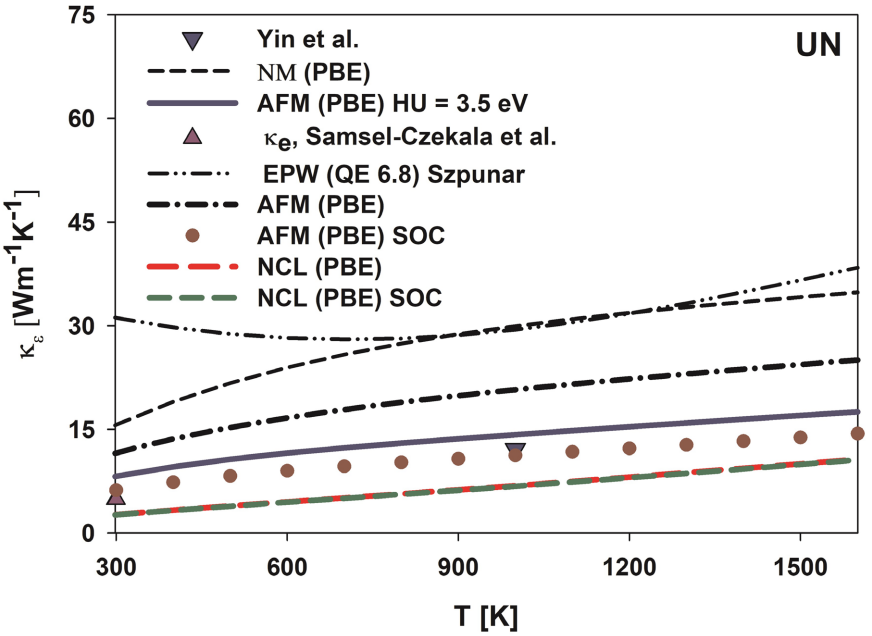

Figure 2. The electronic thermal conductivity (κ_e) of UN calculated previously and indicated by triangle down [26] and up [25] are compared with the calculated using the relaxation time obtained from Equation (1) and combined BoltzTrap2/VASP codes using GGA/PBE calculations for UN: AFM, GGA = HU 3.5 eV (solid dark blue line), AFM GGA + SOC (dark red circles), NM (short-dashed black line) AFM (dashed-dot black line) and NCL magnetism with SOC correction (medium-dashed green line) and without correction (long-dashed red line). The previously listed EPW calculations [11] for NM UN are shown by dashed-dot-dot black line.

3.3. Thermal Expansion

In **Figure 3**, the obtained from Equation (3) linear thermal expansion (α) and the respective experimental correlation [24] for a is presented by open black circles to compare with the calculated results using QHA within DFT [13] [18] [19] for temperatures $0 \leq T \leq 1000$ K: It can be noted that within GGA/PBE DFT only when implementing HU = 3.5 eV correction we get good agreement with experiment. Without this large HU implementation, linear thermal expansion is under-

estimated.

The included in Figure 3 MCTE (green spheres) was calculated using Equation (4) with T_0 temperature set to 303 K and measured lattice constants for UN [27] We also included α (grey triangles up) calculated from the provided parabolic correlation for a [27], which coincide with MCTE at T_0 temperature. These results are much higher due to being measured in oxidative condition as pointed by the authors. We extend the extrapolated correlation for α to zero temperature (although not valid) and note that it is also much higher than the obtained values from DFT/QHA.

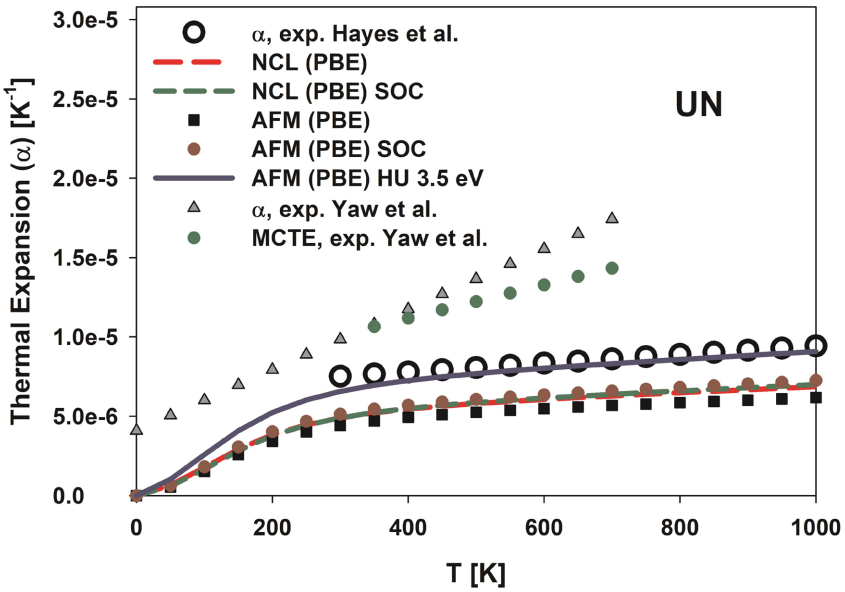

Figure 3. The calculated linear thermal expansion (α) of NCL and AFM UN using GGA/PBE, GGA/PBE + HU = 3.5 eV and GGA/PBE-SOC as indicated in the legend. The experimentally measured α (Hayes *et al.* [24]) is indicated by black solid circles. MCTE (green spheres), calculated using Equation (4) with T_0 temperature set to 303 K and measured lattice constants for UN [27] together with α (grey triangles up) calculated (Equation (3)) up to 0 K temperature for UN in oxidative condition.

We found that to reproduce thermal expansion, calculated using QHA/DFT 5th order polynomial fit (using seven significant figures in trendline) had to be used for the lattice constant as a function of temperature with R^2 = 0.99999433. The respective derived equation for thermal expansion (α) is:

$$\alpha = \left(-5\times 3.7582125\times 10^{-17}T^4 + 4\times 1.2727522\times 10^{-13}T^3 - 3\times 1.6961513\times 10^{-10}T^2 + 2\times 1.1846754\times 10^{-7}T - 5.3854652\times 10^{-6}\right)\Big/ a$$

where a is : (6)

$$a = -3.7582125\times 10^{-17}T^5 + 1.2727522\times 10^{-13}T^4 - 1.6961513\times 10^{10}T^3 + 1.1846754\times 10^{-7}T^2 - 5.3854652\times 10^{-6}T + 4.8828758$$

We used here the scaling factor $\gamma = 0.980859$ to reduce the overestimated lattice constant. This scaling factor does not affect thermal expansion but corrects in the

formula the lattice constant in agreement with the value at 300 K evaluated from experiment by Hayes *et al.* [24]. In Figure 4 one can compare that Equation (6) reproduces very well thermal expansion evaluated using QHA/DFT for UN calculated using GGA + HU = 3.5 eV as implemented in VASP/Phonopy codes, with the exception of faster decrease to 0 K^{-1} at a temperature of 24 K instead of 0 K. However our calculations do not model magnetic phase transition at Neel temperature and therefore we can not make comparison for temperatures below 50 K.

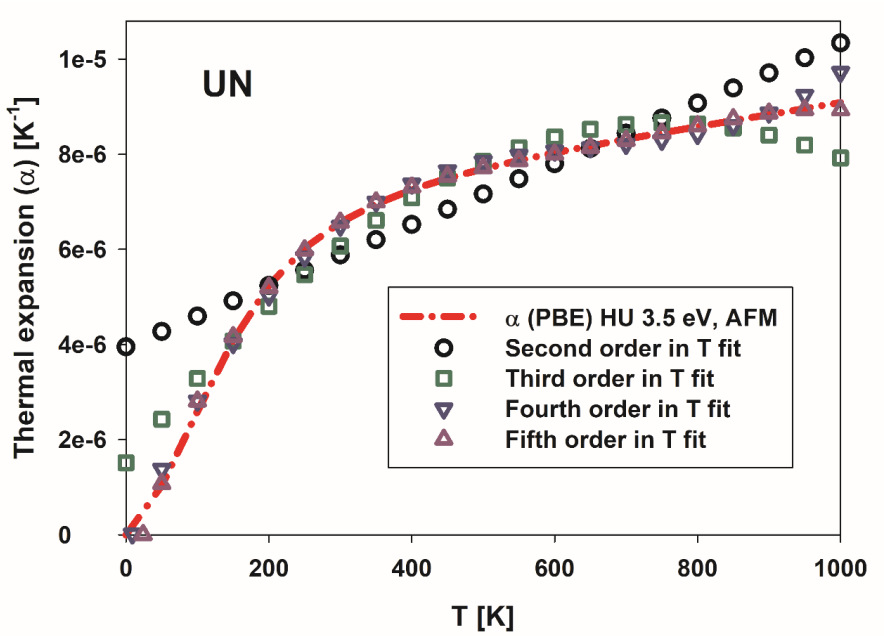

Figure 4. The comparison of thermal expansion calculated using QHA/DFT using GGA + HU = 3.5 eV (dashed dot red line) versus evaluated from polynomial fits to the respective lattice constants as a function of temperature plot. The following fits (done using seven significant figures in trendline label) in used temperature (T) order are shown as indicated: second order (black circles, R^2 = 0.99799604); third order (green square, R^2 = 0.99966980); fourth order (dark grey triangle down, R^2 = 0.99997247) and fifth order (dark pink triangles up, R^2 = 0.9999433).

The fourth order fit (dark grey triangle down) is also in good agreement with the QHA/DFT result except at temperatures of 950 - 1000 K where thermal expansion is overestimated and additionally it goes to 0 K^{-1} at the temperature of 9 K. The second and third order fit cannot reproduce QHA/DFT results as demonstrated in Figure 4.

3.4. Bulk Modulus

In Figure 5, the calculated bulk modulus (BM) using QHA within DFT [13] [18] [19] for temperatures $0 \leq T \leq 1000$ K is shown as indicated. In contrast to previously discussed results, where BM is underestimated with HU correction implemented, we get good agreement with experiment [21] [22] for NCL (long

dashed red line) and AFM UN (black squares) without HU or SOC correction incorporated.

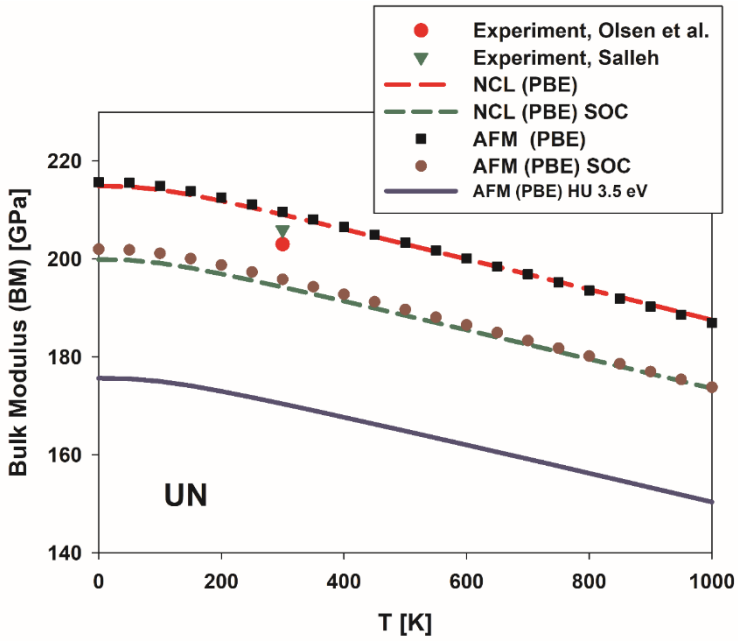

Figure 5. The calculated bulk modulus (*BM*) of nonmagnetic (NM), antiferromagnetic (AFM), and noncollinear (NCL) magnetism in UN using GGA/PBE, GGA/PBE + HU = 3.5 eV and GGA/PBE-SOC as indicated in the legend. The experimentally measured *BM* (Olsen *et al.*, [22], Salleh *et al.*, [21]) are indicated respectively by a red sphere and green triangle up.

4. Summary and Conclusions

An extended exploration of the properties of UN has been performed using density functional theory as implemented in the VASP [13] code and combined with BoltzTrap2 [12] and Phonopy [18] [19] codes.

We found that there is no unique approach within DFT calculations of all properties of UN, which would lead to the best fit with experiment. The best setup depends on the target property.

We have shown that the electronic resistivity and electronic thermal conductivity of the UN can be predicted from first principles in good agreement with the experiment for 1*k* AFM UN using GGA/PBE with either SOC or HU = 3.5 eV correction incorporated (**Table 1** and **Figure 1**, **Figure 2**). It is not surprising that both corrections produced similar results, as they act similarly by splitting free electronic states of DFT into seven 5f orbitals of U atoms, which increases resistivity. The same relaxation time was used that was developed previously for nonmagnetic case using EPW code. Furthermore, we note that, in the other approaches or when using NM or NCL magnetism, overprediction or underprediction of results occurs when comparing with experiment. In particular HU + SOC case for AFM UN was excluded due to significantly overestimated resistivity and therefore reduced electronic thermal conductivity, respectively While the lattice

constant and *BM* are predicted in good agreement with experiment without HU correction (Table 1, Table 2, Figure 5), the respective thermal expansion and *BM'* are significantly underestimated unless HU = 3.5 eV correction is incorporated (Table 2, Figure 3). NM UN with the underestimated lattice constant shows the highest *BM* (Table 2). Both AFM and NCL UN reproduce well experimental *BM* (Table 2) without SOC correction, but lattice constants are in better agreement with experiment with SOC correction included.

Acknowledgements

The authors acknowledge access to high-performance supercomputers at the Digital Research Alliance of Canada (CalculQuebec, WestGrid, and SHARCNET). Free access to BoltzTrap2, Quantum Espresso, EPW codes, and technical support (especially prompt installations by Ata Roudgar and Ali Kerrache) is acknowledged.

The authors acknowledge a constructive discussion with Dr. S. Poncé and a very helpful 2021 EPW workshop.

This work was supported by a Discovery Grant from the National Sciences and Engineering Research Council of Canada.

Author Contributions

B. Szpunar: Conceptualization, developed the theoretical formalism, performed the numerical simulations, visualization, writing.

S. L. Dudarev: Conceptual contribution, review and editing.

Conflicts of Interest

The authors declare no conflicts of interest regarding the publication of this paper.

References

[1] Nuclear Energy Agency (NEA) (2018) State-of-the-Art Report on Light Water Reactor Accident-Tolerant Fuels. Nuclear Science. NEA No. 7317. OECD Publishing, 367.

[2] Pioro, I.L., Khan, M., Hopps, V., Jacobs, C., Patkunam, R., Gopaul, S., *et al.* (2008) SCW Pressure-Channel Nuclear Reactor Some Design Features. *Journal of Power and Energy Systems*, **2**, 874-888. https://doi.org/10.1299/jpes.2.874

[3] Liechtenstein, A.I., Anisimov, V.I. and Zaanen, J. (1995) Density-Functional Theory and Strong Interactions: Orbital Ordering in Mott-Hubbard Insulators. *Physical Review B*, **52**, R5467-R5470. https://doi.org/10.1103/physrevb.52.r5467

[4] Dudarev, S.L., Botton, G.A., Savrasov, S.Y., Humphreys, C.J. and Sutton, A.P. (1998) Electron-Energy-Loss Spectra and the Structural Stability of Nickel Oxide: An LSDA + U Study. *Physical Review B*, **57**, 1505-1509. https://doi.org/10.1103/physrevb.57.1505

[5] Dudarev, S.L., Liu, P., Andersson, D.A., Stanek, C.R., Ozaki, T. and Franchini, C. (2019) Parametrization of LSDA + U for Noncollinear Magnetic Configurations: Multipolar Magnetism in UO_2. *Physical Review Materials*, **3**, Article ID: 083802. https://doi.org/10.1103/PhysRevMaterials.3.083802

[6] Dorado, B., Amadon, B., Freyss, M. and Bertolus, M. (2009) DFT + U Calculations of

the Ground State and Metastable States of Uranium Dioxide. *Physical Review B*, **79**, Article ID: 235125. https://doi.org/10.1103/physrevb.79.235125

[7] Allen, J.P. and Watson, G.W. (2014) Occupation Matrix Control of D- and F-Electron Localisations Using DFT + U. *Physical Chemistry Chemical Physics*, **16**, 21016-21031. https://doi.org/10.1039/c4cp01083c

[8] Bedford, R., Murphy, S., Green, H., Cooper, S., Orr, R., Neilson, W. and Cooper, M.W.D. (2026) Impact of the U Parameter on the Predicted Defect Chemistry of Materials: The Example of $PuO_{2\pm x}$. *Physical Review Materials*, **10**, Article ID: 065403. https://doi.org/10.1103/w8xw-ghmh

[9] Poncé, S., Margine, E.R., Verdi, C. and Giustino, F. (2016) EPW: Electron-Phonon Coupling, Transport and Superconducting Properties Using Maximally Localized Wannier Functions. *Computer Physics Communications*, **209**, 116-133. https://doi.org/10.1016/j.cpc.2016.07.028

[10] Giannozzi, P., Baroni, S., Bonini, N., Calandra, M., Car, R., Cavazzoni, C., *et al.* (2009) Quantum ESPRESSO: A Modular and Open-Source Software Project for Quantum Simulations of Materials. *Journal of Physics: Condensed Matter*, **21**, Article ID: 395502. https://doi.org/10.1088/0953-8984/21/39/395502

[11] Szpunar, B. (2025) DFT Studies of the Effect of Magnetic Ordering and Hubbard U on the Properties of UN. *Journal of Physics and Chemistry of Solids*, **205**, Article ID: 112798. https://doi.org/10.1016/j.jpcs.2025.112798

[12] Madsen, G.K.H., Carrete, J. and Verstraete, M.J. (2018) BoltzTraP2, a Program for Interpolating Band Structures and Calculating Semi-Classical Transport Coefficients. *Computer Physics Communications*, **231**, 140-145. https://doi.org/10.1016/j.cpc.2018.05.010

[13] Kresse, G. and Joubert, D. (1999) From Ultrasoft Pseudopotentials to the Projector Augmented-Wave Method. *Physical Review B*, **59**, 1758-1775. https://doi.org/10.1103/physrevb.59.1758

[14] Szpunar, B., Ranasinghe, J.I., Malakkal, L. and Szpunar, J.A. (2020) First Principles Investigation of Thermal Transport of Uranium Mononitride. *Journal of Physics and Chemistry of Solids*, **146**, Article ID: 109636. https://doi.org/10.1016/j.jpcs.2020.109636

[15] Szpunar, B. (2012) Investigation of Urania within LDA + U Method. *Journal of Physics and Chemistry of Solids*, **73**, 1003-1009. https://doi.org/10.1016/j.jpcs.2012.03.007

[16] Li, G., Liu, N., Qiu, R. and Yuan, H. (2025) Noncollinear 3k-Type Antiferromagnetic Ground State and Multipolar Exchange Interactions in Uranium Nitride. *Physical Review B*, **112**, Article ID: 054442. https://doi.org/10.1103/d8mt-3vmd

[17] Perdew, J.P., Burke, K. and Ernzerhof, M. (1997) Generalized Gradient Approximation Made Simple [Phys. Rev. Lett. 77, 3865 (1996)]. *Physical Review Letters*, **78**, 1396-1396. https://doi.org/10.1103/physrevlett.78.1396

[18] Togo, A., Chaput, L., Tanaka, I. and Hug, G. (2010) First-Principles Phonon Calculations of Thermal Expansion in Ti_3SiC_2, Ti_3AlC_2, and Ti_3GeC_2. *Physical Review B*, **81**, Article ID: 174301. https://doi.org/10.1103/PhysRevB.81.174301

[19] Togo, A., Chaput, L., Tadano, T. and Tanaka, I. (2023) Implementation Strategies in Phonopy and Phono3py. *Journal of Physics: Condensed Matter*, **35**, Article ID: 353001. https://doi.org/10.1088/1361-648x/acd831

[20] Jochym, P.T. and Parlinski, K. (2000) *Ab Initio* Lattice Dynamics and Elastic Constants of ZrC. *The European Physical Journal B*, **15**, 265-268. https://doi.org/10.1007/s100510051124

[21] Salleh, M.D., MacDonald, J.E., Saunders, G.A. and Du Plessis, P.D.V. (1986) Hydrostatic Pressure Dependences of Elastic Constants and Vibrational Anharmonicity of Uranium Nitride. *Journal of Materials Science*, **21**, 2577-2580. https://doi.org/10.1007/bf01114310

[22] Staun Olsen, J., Gerward, L. and Benedict, U. (1985) A New High-Pressure Phase of Uranium Nitride Studied by X-Ray Diffraction and Synchrotron Radiation. *Journal of Applied Crystallography*, **18**, 37-41. https://doi.org/10.1107/s0021889885009736

[23] Hayes, S.L., Thomas, J.K. and Peddicord, K.L. (1990) Material Property Correlations for Uranium Mononitride. *Journal of Nuclear Materials*, **171**, 289-299. https://doi.org/10.1016/0022-3115(90)90376-x

[24] Hayes, S.L., Thomas, J.K. and Peddicord, K.L. (1990) Material Property Correlations for Uranium Mononitride. *Journal of Nuclear Materials*, **171**, 262-270. https://doi.org/10.1016/0022-3115(90)90374-v

[25] Samsel-Czekała, M., Talik, E., de V. Du Plessis, P., Troć, R., Misiorek, H. and Sułkowski, C. (2007) Electronic Structure and Magnetic and Transport Properties of Single-Crystalline UN. *Physical Review B*, **76**, Article No. 14442. https://doi.org/10.1103/physrevb.76.144426

[26] Yin, Q.A., Kutepov, H.K., Haule, K., Kotliar, G., Savrasov, S.Y. and Pickett, W.E. (2011) Electronic Correlation and Transport Properties of Nuclear Fuel Materials. *Physical Review B*, **84**, Article ID: 195111. https://doi.org/10.1103/physrevb.84.195111

[27] Yaw, N.S., Karcher, S., Abdul Hameed, M., Kindall, E.C., van Veelen, A., Wilkins, M.C.D., *et al.* (2025) Thermal Expansion and Degradation of Uranium Mononitride under High-Temperature Oxidative Conditions. *NPJ Materials Degradation*, **9**, Article No. 165. https://doi.org/10.1038/s41529-025-00708-1